Dynamic modeling and simulation of a solar-assisted multi-effect distillation plant

Alberto de la Calle[a,b,*], Javier Bonilla[a], Lidia Roca[a], Patricia Palenzuela[a]

[a]*CIEMAT - Plataforma Solar de Almería, Ctra. de Senés s/n 04200 Tabernas, Almería, Spain*
[b]*Universidad de Almería, Ctra. Sacramento s/n, 04120 Almería, Spain*

Abstract

This paper presents a dynamic model of a solar-assisted multi-effect distillation (MED) plant, carrying on with the previous work "Dynamic modeling and performance of the first cell of a multi-effect distillation plant"[1]. The dynamic model has been designed according to the experience with an experimental solar thermal desalination system erected at CIEMAT-Plataforma Solar de Almería (PSA). The mathematical formulation based on physical principles describes the main heat and mass transfer phenomena in this kind of facilities. The model was implemented using the equation-based object-oriented Modelica modeling language. Based on a modular and hierarchical modeling, different specific-phenomenon submodels have been developed. They have been interconnected between them, thus making a three levels deep hierarchy. All the submodels have been calibrated and validated with experimental data. The numerical predictions show a good agreement with measured data.

Keywords: solar desalination, falling film evaporation and condensation, object-oriented modeling, Modelica

1. Introduction

Water is an essential part of life. The lack of fresh water in areas with high water-stress is one of the most important problems which researchers face. Three-fourths part of The Earth surface is covered by water, but the 97% is salt water. Seawater desalination is one of the possible solutions for coastal regions, but, it requires significant quantities of energy in order to achieve separation of salt from seawater. Coupling desalination plants with renewable energies is a way to reduce the environmental pollution of this process. Solar energy is one of the most promising alternatives since it is usual to find high insolation levels in high water-stress areas [2].

Reverse osmosis (RO), multi-stage flash (MSF) and MED account for more than 94% of the global desalination capacity [3]. Among them, MSF and MED technologies can be coupled with solar thermal systems because most of the energy consumption is thermal energy. Both technologies allow to be coupled in two separated devices, the solar collector and the distiller. MED technology carries on being preferred in most of the large scale solar thermal plants due to its low top brine temperature (TBT), typically less than 80°C, and its low specific energy consumption requirements [4].

*Corresponding author. Tel.:+34 950 387 900; Fax: +34 950 365 300
Email addresses: alberto.calle@psa.es (Alberto de la Calle), javier.bonilla@psa.es (Javier Bonilla), lidia.roca@psa.es (Lidia Roca), patricia.palenzuela@psa.es (Patricia Palenzuela)

The collector is a device which captures the solar radiation and transfers its heat to a fluid. In solar-assisted MED plants, the working fluid is commonly water or synthetic oil and it is usually stored in a thermal storage system [5]. The solar collector or the storage system can be directly connected to the MED unit or indirectly by means of a heat exchanger.

There are many kinds of MED plants, but in all of them, the distillation process is similar. The plant is made up of a series of hermetic elements, called effects, connected between them. At each one, a series of simultaneous evaporation/condensation processes take place in a decreasing sequence of pressures and temperatures. At the first effect, the one with the highest pressure, an external heat source drives the first boiling of the seawater that flows inside. The steam generated within the effect is used as the heat source of the next effect, so, while on one hand, the incoming steam is condensing, on the other, the seawater is boiling, and thus producing additional steam. This process is repeated in each effect [3].

The process model and simulation can provide insight about the physical phenomena and give detailed information about the performance that may be useful in order to improve the efficiency of the plant over a wide range of operating conditions without experimentation in the real plant. Several steady-state models have been published covering a wide variety of plant configurations. Some of the most recent contributions in this area have been done by Kouhikamali who studied the influence of different configurations of feed water preheating [6], Joo and Kwak who increased the mechanical efficiency and economical profit of a MED system [7] or Palenzuela et al. who evaluated different cooling technologies of concentrated solar power plants and their combination with desalination processes (RO and MED) [8]. The contributions made by El-Nashar [9, 10] and Palenzuela et al. [11] deserve special attention because they validated their respective models with experimental data.

The literature related to dynamic modeling is scarce. However, the interest for this kind of modeling has grown recently. Kishore et al. [12] presented a work-in-progress simulator for the steady state and the dynamics of a multi-effect distillation mechanical vapour compression (MED-VC) desalination system, showing a dynamic simulation of a single effect. Roca et al. [13] developed a dynamic model of a multi-effect distillation plant based on the heat transfer correlations presented in [14]. This model is an improved version of a previous one in which the heat transfer coefficients were considered constants [15]. It was developed with the object-oriented Modelica language and its main purpose was the prediction of the thermal dynamics of the heater and the distillate production rate. Kim et al. [16] presented a simulation model for predicting transient behavior of a solar-assisted MED plant. The model, which was focused on the long-term thermal and performance analysis, includes an evacuated-tube collector, a plate heat exchanger, storage tanks and a MED plant. This model has been used by Thu et al. [17] in the study of a suitable configuration for a hybridization between adsorption desalination (AD) and MED processes.

The present paper carries on the work started in [1] where the focus was on the modeling of the first effect of a solar-assisted MED plant. Using an object-oriented modeling methodology, the model presented was divided into submodels that encapsulated and covered the dynamics of each one of the subprocesses that take place in the system. Reusing part of this work and following with this modeling methodology, a new dynamic model of a MED plant has been developed in order to study its performance in different scenarios and design operating strategies to improve its efficiency. This non-linear first principles model has been implemented with the object-oriented Modelica language. The model uses as inputs the natural inputs of the system, i.e., the hot water flow, the inlet seawater flow and the ambient temperature. The model is based on the AQUASOL experimental solar desalination system [18] and it has been calibrated and validated with experimental data. The model predicts the transient thermal behavior of each effect and its low computational effort allows fast simulation for control purposes.

2. Description of the plant

In 1987, a MED unit manufactured by ENTROPIE was erected at CIEMAT-Plataforma Solar de Almería with the aim of testing and developing the solar thermal MED process. Since then, the original experimental solar desalination system has been undergone several changes until becoming a 24-h operation hybrid solar-gas desalination system (v. Fig. 1) that tries to meet at the same time the requirements of low-cost, high efficiency and zero liquid discharge [18]. The current system is flexible regarding the energy supply of the MED plant, it can be thermal-fed by a compound parabolic collector (CPC) solar field, by a propane gas boiler by means of a double effect absorption heat pump (DEAHP) or in a hybrid mode by both. The DEAHP is coupled with the last effect of the MED plant recovering part of its low-temperature energy. This energy is injected to the MED plant directly or through the tanks indirectly at high temperature [19].

The distillation unit is a forward-feed vertically stacked MED plant with 14 cells (v. Fig. 2). In 2005 under the framework of the AQUASOL project, the original first effect was replaced with a new one able to work with hot water coming either from the thermal storage tanks or from the DEAHP. The hot water inlet temperature can vary between 57-75 °C, exhibiting low deviations in the overall performance ratio [20]. This temperature can be controled with a three-way valve placed between the hot tank and the MED plant. The inlet flow rate can range between 7-12 L/s.

Besides the first and the last cells, the remaining cells are identical. Every cell is composed of an effect and a preheater, two horizontal tube bundles, where, over the first one, seawater evaporation is produced and, over the second one, part of the vapor is condensed. Fig. 3 shows a schematic cross section of a cell. The first effect is a square-pitch bundle and hot water flows inside the tubes crossing the evaporator four times in a highly turbulent flow [1]. The last cell preheater, also called condenser, is much bigger than the other preheaters.

A flow diagram of the plant is depicted in Fig. 4. A great amount of seawater is pumped to the condenser placed next to the 14^{th} effect which is used to condense the vapor generated in such effect. Seawater is also used for preserving the pressure inside, however, there is not an specific control system for this purpose. Using a three way valve, part of this seawater is rejected and the remaining part is used to feed the plant. The feed seawater flow rate, that can vary between 6-8 m^3/h, is preheated while flows through every cell, and finally, it is spilt inside the plant in the 1^{st} cell. Here, seawater is sprayed over the effect where hot water flows inside the tubes transfering heat. When the spray reaches the first row of the tube bundle, a thin film of seawater is formed over each tube surface. The seawater in the film flows downward due to the gravitational force, falling over all the column tubes. Part of seawater evaporates in the effect and the remaining part, with higher salt concentration, falls over the next effect. The vapor produced at the effect flows to the preheater located next to it. A wire mesh demister prevents brine droplets from reaching the preheater tube bundle. When condensation is produced over the tube surface, a thin film of water is formed. This film slides down due to the gravitational force and it falls over all the column tubes increasing their thickness as more vapor condenses on the film. Seawater flows inside the tubes, acquiring heat from the condensation. The distillate and the vapor, which has not condensed, flow to inside the horizontal tube bundle of the next effect. This mixture is used to heat the high concentrated seawater coming from the 1^{st} effect where this process is repeated.

The decreasing pressure arrangement provides an efficient heat transfer between the vapor-distillate mixture and the seawater coming from the previous effect because the difference between the saturation temperatures of seawater and vapor at same pressure is not large enough. When seawater enters to the effect, the pressure drop between effects produces flash evaporation which in turn decreases the

seawater temperature before covering the surface of the tubes. For this reason, seawater is always at lower temperature than the water which flows inside the tubes.

The vapor condensed at each effect, each preheater and the distillate produced at the final condenser make up the total distillate production of the plant. Part of sensible heat of the distillate is recovered by the plant when flows inside the tube bundle of the effects. With the purpose of improving the process at PSA-MED plant, the distillate accumulated in one preheater is added to the distillate produced in the effect and flow to the next effect with the exception of the 4^{th}, 7^{th}, 13^{th} and 14^{th} cells as it is shown in Fig. 4. In the 4^{th} cell the distillate is divided, one part flows to the 7^{th} cell and the remaining part flows to the 10^{th} cell where it is mixed with the extraction of the 7^{th} cell. This mixture flows to the 10^{th} and 13^{th} cells. The distillate accumulated in the 10^{th} cell is mixed with the extracted from the 7^{th} cell and divided again, one part flows to 13^{th} cell and the remaining together with the distillate from the 13^{th} and 14^{th} cells flows to the condenser where part is evaporated by a flash process.

The salt water for the desalination plant is obtained by brackish water wells from Tabernas Dessert whose salinity is 0.3326%. The MED plant is operated in a close circuit. Two pools are used to store all the seawater: a small pool is used to mix the distillate and the brine rejected and a bigger one for the supply of the plant. The cooling seawater is spilt into the big pool and part of the heat released by the condenser could increase its temperature during a experiment. To avoid that, a dry cooler is switched on, however sometimes it is insufficient [11]. Therefore, it is difficult to obtain a long-steady state in all its variables even though the MED plant has control mechanisms at its inputs.

The MED plant has a vacuum system in order to remove the air and the non-condensable gases generated during the desalination process. It consists in two hydro-ejectors which are connected to the 2^{nd} and 7^{th} effects and to the final condenser. This system removes the gases at the beginning of the experiment, being water vapor the only gas inside the effects. The hydro-ejectors are within a closed circuit with a tank and an electric pump that drives seawater through the ejectors at a pressure of 3 bar [11].

The current design specifications of the MED plant are shown in Table 1 [11]. All the tube bundles are made of 90-10 Cu-Ni with a 14 mm of outside diameter. The heat transfer areas are:

- 1^{st} effect: 24.26 m^2
- 2^{nd}-14^{th} effect: 26.28 m^2
- Preheater: 5 m^2
- Condenser: 18.3 m^2

3. Subsystem Modeling

In §1, it is mentioned that modeling and simulation is a powerful methodology to improve the efficiency of processes. This is because simulations can predict the plant behavior over different design operating conditions. Due to the complexity of this process, it is important to identify and model each one of the subprocesses in order to cover all the dynamics with enough detail. The object-oriented modeling methodology allows to encapsulate each one of these subprocesses into submodels. The general model is composed of these submodels.

The model has been implemented with the non-proprietary Modelica language [21]. This modeling language allows to formulate the problems in an acausal way, being well suited for representing physical

systems. Moreover, Modelica is an object-oriented language, therefore, each component diagram can be encapsulated in a class and hierarchical structures can be created.

Three levels are enough to develop the model of the MED plant. The low level cover each subprocess of heat and mass transfer of the system, the medium level assembles subsystems dealing with its usefulness, and the high level composes the complete model of the plant.

In computational fluid dynamics, the procedure to calculate the thermodynamic properties has a great influence on the error and on the computational time [22]. There are several problems related with dynamic models that are directly caused by the computation scheme applied to them. With respect to the models described in this section, the industrial formulation for thermodynamic properties of water and steam [23] has been used in the models with water and vapor. For the models with seawater, the properties has been calculated with the formulation proposed by Sharqawy et al. [24] and the inverse functions presented in [1].

The details of all variables used in this section are described in the nomenclature.

3.1. Low level

3.1.1. Falling film condenser

Mostly, condensation happens over surfaces whose temperature is lower than the saturation temperature. At falling film condensers, like the preheaters of PSA-MED plant, when condensation appears a thin film of water grows over each tube surface. This film slides down under gravitational force and falls over all the column of tubes increasing their thickness because more vapor condenses over the film. The film thickness determines the mass and heat flow rates.

Based on the model presented in [1], the model showed in Fig. 5(a) determines, by an algebraic procedure, the distillate production using only one control volume (CV). The heat transfer between the tube and the condensate is calculated according to the Nusselt film condensation theory and the Newton's law of viscosity [25]. An average temperature of the film between vapor saturation temperature at the vapor-film interface and the tube temperature at the surface is assumed. Also, it is considered that the film drains smoothly over the tube below. With these assumptions, the average heat transfer coefficient can be calculated as follows [26]:

$$\bar{\alpha}_c = 0.729 \left(\frac{\rho_c(\rho_c - \rho_{c,sv}) g k_c^3 L_c^*}{2\mu_c(T_{c,sl} - T_{c,w}) r_c N_{c,row}} \right)^{1/4}, \tag{1}$$

where the modified latent heat of vaporization is defined as:

$$L_c^* = L_c + 0.68 C_{p,c}(T_{c,sl} + T_{c,w}). \tag{2}$$

The total condensation rate by the tube bundle is determined by the Newton's law of cooling:

$$\dot{m}_{c,cond} = \frac{\dot{Q}_{c,w}}{L_c^*} = \frac{\max(0, N_{c,col} N_{c,row} \bar{\alpha}_c A_{c,w}(T_{c,sl} - T_{c,w}))}{L_c^*}. \tag{3}$$

The max function guarantees a condensation rate only when the wall temperature is lower than the saturation temperature.

3.1.2. Horizontal tube bundle condenser

Inside the horizontal tube bundle of each effect a vapor-distillate mixture coming from the previous effect releases its latent heat and part of its sensible heat in order to evaporate the seawater that flows over the outer surface. The decreasing pressure arrangement of the effects guarantees that the tube temperature is lower than the saturation temperature of the incoming vapor. When the vapor condenses at the inner surface of the tube, a thin film of water grows covering this surface. The liquid film drains downwards due to the gravitional force and it becomes more bulky at the bottom of the tube than at the top. A stratified liquid layer is formed at the bottom of the tube and flows axially. While the distillate crosses the tube, it transfers part of its sensible heat since the tube temperature is lower than the temperature of the distillate. A detailed analysis of condensation inside tubes is complicated because factors like the vapor velocity and the rate of liquid accumulation on the walls of the tubes strongly influence the process.

As the model of the falling film condenser §3.1.1, the model of the horizontal tube condenser (v. Fig. 5(b)) assumes an average heat transfer coefficient. If the heat transfer at the bottom of the tube is negligible compared to the upper portion of the tube, and the void fraction (and hence the interfacial area) does not vary significantly along the tube, Chato [27] recommends this expression:

$$\bar{\alpha}_{bc} = 0.555 \left(\frac{\rho_{bc}(\rho_{bc} - \rho_{bc,sv}) g k_{bc}^3 L_c^*}{2\mu_{bc}(T_{bc,sl} - T_{bc,w}) r_{bc} N_{bc,row}} \right)^{1/4}. \tag{4}$$

Eq. 2 and Eq. 3 are used to obtain the total condensation rate over the tube bundle. The condensate has an average temperature between the vapor saturation temperature and the tube temperature.

During the normal operation of the plant, it has been observed that the vapor of one effect never reaches the next effect crossing the condenser, therefore, the model avoid this situation assuming only liquid as output. The dynamics of the accumulation of liquid in the condenser are neglected. The mass balance is:

$$0 = \dot{m}_{bc,in} - \dot{m}_{bc,out} + \dot{m}_{bc,cond}. \tag{5}$$

Due to the low flowing speed of the distillate across the tube, the model assumes that when the distillate leaves the condenser it has the tube surface temperature. The transfer of this sensible heat is calculated according to:

$$\dot{Q}_{bc,w2} = \dot{m}_{bc,cond} h_{bc,ff} + \dot{m}_{bc,in} h_{bc,in} - \dot{m}_{bc,out} h_{bc,w}. \tag{6}$$

The total heat flow rate transfered to the wall tube is the sum of the contributions related to the latent and the sensible heat.

3.1.3. Falling film evaporator

In a falling film evaporator the liquid is sprayed over the first row of the tube bundle. Over the surface of these tubes a thin film of liquid is formed and it falls over the tubes below. The tube surface is at higher temperature than the saturation temperature, therefore, part of the film evaporates. The mass and heat transfer rates are determined by the film thickness, but it changes with the tangential direction of the tube and with the position of the tube in the column. An analitycal solution for this problem is more complex than needed. There are many factors which affect the thickness and this is the reason why several authors have published Nusselt number correlations for falling films evaporators [28]. Among them, Sernas [29] and Rogers et al. [30] propose Eq. 7 for horizontal tube bundles with different values for the coefficients. This correlation with coefficients adjusted with real data of the plant is used in this model.

$$Nu_e = n_1 Re_e^{n_2} Pr_e Ar_e^{n_3}. \tag{7}$$

The evaporator model (v. Fig. 5(c)) used in this work was presented in [1]. It is an algebraic lumped model where an average film thickness and average thermodynamic properties for the whole tube bundle are assumed and where the stuckle mass effect is neglected.

The mass and energy balances are:

$$0 = \dot{m}_{e,in} - \dot{m}_{e,out} - \dot{m}_{e,ev}, \tag{8}$$

$$0 = \dot{Q}_{e,w} + \dot{m}_{e,in} h_{e,in} - \dot{m}_{e,out} h_e - \dot{m}_{e,ev} h_{e,sv}. \tag{9}$$

The evaporated mass flow rate is:

$$\dot{m}_{e,ev} = \frac{\max(0, \dot{Q}_{e,w} + \dot{m}_{e,in}(h_{e,in} - h_{e,sl}))}{h_{e,sv} - h_{e,sl}}. \tag{10}$$

The outlet mass fraction is:

$$S_{e,out} = \frac{\dot{m}_{e,in} S_{e,in} - \dot{m}_{e,ev}}{\dot{m}_{e,in} - \dot{m}_{e,ev}}. \tag{11}$$

The heat flow rate is:

$$\dot{Q}_{e,w} = N_{e,col} N_{e,row} \bar{\alpha}_e A_e (T_{e,sl} - T_{e,w}). \tag{12}$$

The definition of Nusselt number allows to calculate the average heat transfer coefficient:

$$Nu_e = \left(\frac{\bar{\alpha}_e}{k_e} \right) \left(\frac{\nu_e^2}{g} \right)^{1/3}. \tag{13}$$

3.1.4. Pipe

The heat transfer to the liquid flowing through a tube is a phenomenon thoroughly studied. Several Modelica libraries includes pipe models that has been tested with good results like Modelica.Fluid [21] or the MMBs library [31]. Nonetheless, the computational effort that entails to connect fourteen pipe models in series has forced to developed a new pipe model simplifying the previous models. The new model (v. Fig. 5(d)) is a lumped model with one CV.

The proposed balances of mass and energy:

$$0 = \dot{m}_{pp,in} - \dot{m}_{pp,out}, \tag{14}$$

$$\frac{\rho_{pp,av} V_{pp}}{2} \left(\dot{h}_{pp,in} + \dot{h}_{pp,out} \right) = \dot{Q}_{pp,w} + \dot{m}_{pp,in} h_{pp,in} - \dot{m}_{pp,out} h_{pp,out}. \tag{15}$$

All properties of the liquid are evaluated at the average specific enthalpy:

$$h_{pp,av} = \frac{h_{pp,in} + h_{pp,out}}{2}. \tag{16}$$

The heat transfer between the tube surface and the fluid is calculated with the Newton's law of cooling:

$$\dot{Q}_{pp,w} = N_{pp,col} N_{pp,row} \bar{\alpha}_{pp} A_{pp,w} \left(T_{pp,w} - T_{pp,av} \right), \tag{17}$$

where the heat transfer coefficient is given by the Dittus-Boelter Nusselt number correlation [32]:

$$Nu_{pp} = 0.023 Re_{pp}^{0.8} Pr_{pp}^{0.4}. \tag{18}$$

The Reynols number is determined considering the number of parallel pipes:

$$Re_{pp} = \frac{4\dot{m}_{pp,in}}{\pi D_{i,pp}\mu_{pp,av}N_{pp,par}}. \tag{19}$$

Besides the first pipe, the inlet specific enthalpy of the fluid in the pipes and its derivative are given by the output of the previous pipe. At the first pipe, the inlet specific enthalpy is one of the inputs of the system, and its derivative needs to be explicitly calculated together with this input. In order to speed up the simulation, this calculation may be performed offline.

3.1.5. Wall

The wall model (v. Fig. 5(e)) is the element that exchanges heat between the inner and outer sides of the tubes. Considering that the thickness of the tube is 0.7 mm and the 90-10 Cu-Ni alloy has a high thermal conductivity, the conduction across the tube can be neglected. A single wall temperature for the whole tube bundle is assumed:

$$\dot{Q}_{ff,w} - \dot{Q}_{pp,w} = m_w C_{p,w}\dot{T}_w. \tag{20}$$

3.1.6. Flash

Flash evaporation is the partial or total vaporization that occurs when liquid gets inside a vessel where the pressure is lower than its saturation pressure. The liquid suddenly evaporates until both pressures are the same. The released latent heat is used to reduce the temperature of the liquid. This process usually happens when seawater flows from one effect to the next, or when the distillate reaches the condenser.

The flash model (v. Fig. 5(f)), also presented in [1], was developed using a single CV without mass or energy storage and where the latent heat from evaporation is used to cool the seawater down until the saturation temperature is reached.

The evaporated mass flow rate is determined by:

$$\dot{m}_{fl,ev} = \frac{\max(0, \dot{m}_{in}(h_{fl,in} - h_{fl,sl}))}{h_{fl,sv} - h_{fl,sl}}. \tag{21}$$

Where the energy and mass balances are:

$$0 = \dot{m}_{fl,in} - \dot{m}_{fl,out} - \dot{m}_{fl,ev}, \tag{22}$$

$$0 = \dot{m}_{fl,in}h_{fl,in} - \dot{m}_{fl,out}h_{fl,out} - \dot{m}_{fl,ev}h_{fl,sv}. \tag{23}$$

If the liquid is seawater, the outlet mass fraction is obtained from a expression similar to Eq. 11.

3.1.7. Gas volume

The vapor generated at the effect fills all the volumen available inside the cell. The gas pressure is required by all the processes that happen in the cell.

This model, based on the model presented in [1], assumes a homogeneous distribution of the vapor inside the cell. The volume is assumed constant because the liquid phase volume of the cell is negligible if it is compared with the gaseous phase volume. The pressure is calculate with the ideal gas law:

$$p_g V_g = m_g K T_g. \tag{24}$$

The temperature of the gas is the saturation temperature of the water at this pressure. This bond between the temperature and the pressure causes an algebraic loop that is efficiently solved by the simulation environment.

The mass is determinated by the following mass balance:

$$\dot{m}_g = \dot{m}_{g,in} - \dot{m}_{g,out}. \tag{25}$$

3.1.8. Mixer

The mixer is the element that divides the flow from the extractions of distillate at the 7^{th}, 10^{th} and 13^{th} cells. As the model presented in [14], the distillate is proportionally divided.

$$0 = \dot{m}_{mix,in} - y\dot{m}_{mix,out1} - (1-y)\dot{m}_{mix,out2}. \tag{26}$$

3.1.9. Valve

The seawater at the outlet of the condenser is divided by a mass-flow-rate-controlled valve. The feed seawater mass flow rate is provided as input and the valve model determines the cooling seawater rejected.

3.2. Medium level

3.2.1. Heater

The heater model, depicted as a compact model in Fig. 6(a), wraps the main physical phenomenon that takes place on the 1^{st} effect or heater. These phenomena have been described in §3.1. The arrangement of the model is shown in Fig. 7(a). This model is composed by a pipe, a wall, an evaporator and a flash submodels connected together. In order to consider the heat losses to the environment, the wall model can be connected from the outside by means of the heat transfer connector *Q_env*. The hot water line crosses the heater model from the *hw_in* to the *hw_out* fluid connectors releasing its sensible heat from the pipe model to the wall model. The wall model transfers this heat to the falling film evaporator model. The seawater line goes into the heater from the *sw_in* connector, and leaves it, after crossing the flash and evaporator models, by the *sw_out* connector. The vapor produced at flash and evaporator models is collected in the *v_out* connector.

3.2.2. Effect

In a similar way to the heater model, the effect model is also composed by the submodels presented in §3.1. Fig. 6(b) wraps the arrangement shown in Fig. 7(b). The seawater line, just as in the heater model, crosses the effect from the *sw_in* connector to the *sw_out* connector going through of the flash and evaporator models. The vapor generated in these submodels is collected by the *v_out* connector. The heat source in this case is the horizontal tube bundle condenser which transfers the sensible heat of the incoming distillate (*dis_in*) and the latent heat of the vapor coming from the previous cell (*v_in*). The distillate produced in the condenser leaves the effect through the *dis_out* connector. The heat is exchanged between the condenser and the evaporator by means of the wall submodel.

3.2.3. Preheater

The preheater model, Fig. 6(c), constructed as shown in Fig. 7(c), allows heat transfer between a vapor volume, which condenses outside of a tube bundle, and a seawater flow. The gas volume model manages the vapor of the cell. The vapor enters from the *v_in* connector and leaks in the *v_out* connector. Part of the vapor is consumed by the falling film condenser producing distillate that leaves the preheater though the *dis_out* connector and heat that is transfered to the pipe model through the wall model. The seawater line goes into the preheater model from the *sw_in* connector and leaves it though the *sw_out* connector after being heated in the pipe model.

3.2.4. Condenser

The final condenser behaves like a big preheater where all the distillate produced in the plant is collected. The model (v. Fig. 6(d)) is constructed as Fig. 7(d) shows. All the distillate of the plant enters the condenser though the *dis_in* connector. A flash model divides the flow, part is evaporated and goes to the gas model, and part is added to the distillate produced by the falling film condenser which is collected in the *dis_out* connector. The *v_in* connector provides the vapor coming from the effect. The falling film condenser releases the latent heat of the vapor which is transfered through the wall model to the seawater line by means of the pipe model. This line goes into the condenser from the *sw_in* connector to the *sw_out* connector. The derivative of the inlet specific enthalpy can be provided by the *dsw* connector.

3.3. High level

The final arragement of the model is despicted in Fig. 8. The connections of the submodels have been performed as shown in Fig. 4. The model is fed at 14^{th} cell by a fluid source which provides the seawater with a constant salinity of S=0.003326, and, mass flow rate and temperature obtained from experimental data. The three-way valve divides the seawater flow at the exit of the final condenser where part is rejected and goes to the pool and the remaining part is used to feed the plant. This split is controled by the feed seawater mass flow rate signal. A fluid source provides the heater with hot water whose mass flow rate and temperature are experimentally obtained. A convection model calculates the heat losses of the plant to the enviroment. The derivative of the inlet specific enthalpy of the hot water and seawater inputs are provided in order to improve the efficiency of the model. Three sink models are used to establish the outlet boundary conditions.

4. Simulation

Dymola 2015 [33] was the Modelica tool used for the simulation of the mathematical models previously introduced in §3. The numerical solver used was DASSL [34] where the absolute and relative tolerance was set to 10^{-4}. A common laptop, Intel i5 hyper-threading dual-core processor with 8 Gbytes of RAM, was the machine used for the simulations.

The experimental measures used as inputs in the simulations were (v. Fig. 4):

- Inlet hot water mass flow rate (*Fh1*)
- Inlet hot water temperature (*Th0*)
- Inlet feed seawater mass flow rate (*Ff0*)
- Inlet feed and cooling seawater mass flow rate (*Fc0*)
- Inlet feed and cooling seawater temperature (*Tc0*)
- Ambient temperature (*Tamb*)

The derivatives of the specific enthalpy of the hot water and seawater were numerically estimated by the first order backward difference formula.

Although every variable calculated in the model can be considered as an output, the most relevant are the following:

- Outlet hot water temperature (*Th1*)

- Outlet distillate mass flow rate (*Fd0*)
- Outlet condenser seawater temperature (*Tf0*)
- Pressure at the final condenser (*P14*)

The calibration and validation were accomplished with data from the experiments performed the 14^{th} and 18^{th} October 2013 respectively. In these experiments, the plant was only operated in the solar mode and the inputs were varied over all the operation range. The measured data were filtered by a low-pass filter with a cutoff frequency of $2 \cdot 10^{-2}$ Hz in order to reduce the noise in the signals. The calibration was carried out by parts (heater, effect, preheater, condenser and MED models) using the Modelica Optimization library [35].

The model has 57 continuous time states (cts): the wall temperature of heater, effects, preheaters and condenser (28 cts), the mass of the gas volume of preheaters an condenser (14 cts), the outlet specific enthalpy of the pipe of preheaters and condenser (14 cts), and the outlet specific enthalpy of the pipe of heater (1 cts). All of them must be correctly initializated. A complety initialization in steady-state initial conditions in practice is not posible because the model requires to start the simulation with non-zero mass flow rates and the state equations are entanglement. The following guideline has been used for the initialization: the wall temperatures have been initializated in steady-state conditions ($\dot{T}_w = 0$), the gas volume masses have been initializated according to a lineal arrangement of pressures between the 1^{st} and the 14^{th} cells using the experimental measures (*P1-P14*) as references, the outlet specific enthalpy of seawater at the preheaters are initialized according to a lineal arrangement of temperatures between the 1^{st} and the 13^{th} cells using experimental measures (*Tf-Tf1*), the outlet specific enthalpy of seawater at the final condenser is initialized according to the measured temperature (*Tf0*) and the outlet specific enthalpy of the hot water at the heater is initialized according to the measured temperature (*Th1*).

The CPU-time for integration was 10.8 s for the 17000 s simulated. The simulation did not presented state events and the maximum order of integration used be the numerical integrator 3.

Fig. 9 and 10 show the simulation results of the validation day. The simulation begins when the experimental plant operation has been started, and the hot water and feed and cooling seawater have non-zero mass flow rates at both inputs. Along the experiment, their values change several times abruptly covering almost all the operation range of the plant, as it is shown in Fig. 9(a). For the same reason, the inlet hot water temperature also changes several times (v. Fig. 9(b)). The remaining inputs, the ambient temperature and the inlet seawater temperature, are uncontrolled variables and may change with time. The variation of them is shown at Fig. 9(c).

At the beginning of the simulation, it can be observed small spikes in the model response with respect to the measured variables. The cause of them is a small difference between the proposed initial values of the continuous time states and the real values. Outlet hot water and outlet condenser seawater temperatures show good agreements with respect to experimental data (cf. Fig. 9(b) and 9(c)). Although the absolute error exceeds the uncertainty range of the measurement instruments in certain occasions, 0.85 °C, the average error reveals the goodness of fit obtained with the model since it is lower than the uncertainty range, 0.65 and 0.81 °C respectively. The distillate mass flow rate and the pressure of the condenser show higher deviations with respect to experimental data. Nevertheless, the uncertainty range at these two measures is barely higher than the measured value. The average absolute error are 0.0458 kg/s and 8.0 mbar respectively.

5. Conclusions

A new dynamic model of a solar-assisted MED plant has been developed. It is based on physical principles and using object-oriented modeling methodology, the non-lineal model predicts the thermal behavior of the plant. The main subprocesses that take place at the plant have been identified and modeled. Each one of them has been modeled in a self-sufficient component making up a library of submodels. Three levels of detail have been enough to develop the model: the low level is used to cover each subprocess of heat and mass transfer of the system, the medium level is used to assemble subsystems, and the high level is used to compose the complete model of the plant. The MED model uses as inputs the natural inputs of the system, i.e., the hot water flow, the inlet seawater flow and the ambient temperature. The model has been developed using the object-oriented Modelica language and it has been calibrated and successfully validated against experimental data from the PSA solar thermal desalination plant. A good agreement between simulation results and experimental data is obtained where the simulation average error is lower than the uncertainty range of the measurement instruments.

The model covers the whole operation range of the plant and it can be used to study the plant performance in different scenarios and operating strategies to optimize future operating control strategies. The assumptions considered allows fast simulation useful for testing control algorithms. To develop a control system to optimize the energy consumption of the plant is one of the short-term aims. Another goal is to improve the response of the model with new assumptions which do not penalize the computational time.

Acknowledgments

The authors would like to thank to CIEMAT research center, Spanish Ministry of Economy and Competitiveness and ERDF funds for financing this work under the National Plan Project, Predictive control techniques for efficient management of renewable energy microgrids. (POWER), DPI2010-21589-C05-02.

References

[1] A. de la Calle, J. Bonilla, L. Roca, P. Palenzuela, Dynamic modeling and performance of the first cell of a multi-effect distillation plant, Appl Therm Eng 70 (2014) 410–420.

[2] S. Kalogirou, Seawater desalination using renewable energy sources, Prog Energ Combust 31 (2005) 242–281.

[3] C. Li, Y. Goswami, E. Stefanakos, Solar assisted sea water desalination: A review, Renew Sust Energ Rev 19 (2013) 136–163.

[4] M. T. Ali, H. E. Fath, P. R. Armstrong, A comprehensive techno-economical review of indirect solar desalination, Renew Sust Energ Rev 15 (2011) 4187–4199.

[5] H. M. Qiblawey, F. Banat, Solar thermal desalination technologies, Desalination 220 (2008) 633–644.

[6] R. Kouhikamali, Thermodynamic analysis of feed water pre-heaters in multiple effect distillation systems, Appl Therm Eng 50 (2013) 1157–1163.

[7] H.-J. Joo, H.-Y. Kwak, Performance evaluation of multi-effect distiller for optimized solar thermal desalination, Appl Therm Eng 61 (2013) 491–499.

[8] P. Palenzuela, G. Zaragoza, D. C. Alarcón-Padilla, J. Blanco, Evaluation of cooling technologies of concentrated solar power plants and their combination with desalination in the mediterranean area, Appl Therm Eng 50 (2013) 1514–1521.

[9] A. M. El-Nashar, Predicting part load performance of small MED evaporators-a simple simulation program and its experimental verification, Desalination 130 (2000) 217–234.

[10] A. M. El-Nashar, Validating the performance simulation program "SOLDES" using data from an operating solar desalination plant, Desalination 130 (2000) 235–253.

[11] P. Palenzuela, D. C. Alarcón-Padilla, G. Zaragoza, J. Blanco-Gálvez, M. Ibarra, Parametric equations for the variables of a steady-state model of a multi-effect desalination plant, Desalin Water Treat 51 (2013) 1229–1241.

[12] G. Kishore, S. Nisan, S. Dardou, A. K. Adak, V. K. Srivastava, P. K. Tewari, Development of a dynamic simulator (INFMED) for the MED/VC plant, Desalin Water Treat 21 (2010) 364–374.

[13] L. Roca, L. J. Yebra, M. Berenguel, A. de la Calle, Dynamic modeling and simulation of a multi-effect distillation plant, in: Proc. 9th International Modelica Conference, Munich, Germany, 2012, pp. 883–888.

[14] P. Palenzuela, D. C. Alarcón-Padilla, J. Blanco-Gálvez, E. Guillén, M. Ibarra, G. Zaragoza, Modeling of the heat transfer of a solar multi-effect distillation plant at the Plataforma Solar de Almería, Desalin Water Treat 31 (2011) 257–268.

[15] L. Roca, L. J. Yebra, M. Berenguel, D. C. Alarcón-Padilla, Modeling of a Solar Seawater Desalination Plant for Automatic Operation Purposes, J Sol Energy Eng 130 (2008) 041009–1–041009–8.

[16] Y.-D. Kim, K. Thu, A. Myat, K. C. Ng, Numerical simulation of solar-assisted multi-effect distillation (SMED) desalination systems, Desalin Water Treat 51 (2013) 1242–1253.

[17] K. Thu, Y.-D. Kim, G. Amy, W. G. Chun, K. C. Ng, A synergetic hybridization of adsorption cycle with the multi-effect distillation (MED), Appl Therm Eng 62 (2014) 245–255.

[18] D. C. Alarcón-Padilla, J. Blanco-Gálvez, L. García-Rodríguez, W. Gernjak, S. Malato, First experimental results of a new hybrid solar/gas multi-effect distillation system: the AQUASOL project, Desalination 220 (2008) 619–625.

[19] P. Palenzuela, L. Roca, G. Zaragoza, D. Alarcón-Padilla, L. García, A. de la Calle, Operational improvements to increase the efficiency of an absorption heat pump connected to a Multi-Effect Distillation unit, Appl Therm Eng 63 (2014) 84–96.

[20] P. Fernández-Izquierdo, L. García-Rodríguez, D. C. Alarcón-Padilla, P. Palenzuela, I. Martín-Mateos, Experimental analysis of a multi-effect distillation unit operated out of nominal conditions, Desalination 284 (2012) 233–237.

[21] Modelica Association, Modelica Specification 3.3, 2014. URL: `www.modelica.org/documents`.

[22] M. Kunick, H.-J. Kretzschmar, U. Gampe, Fast Calculation of Thermodynamic Properties of Water and Steam in Process Modelling using Spline Interpolation, in: Proc. ICPWS XV, Berlin, Germany, 2008, p. 5.

[23] IAPWS, Release on the IAPWS, Industrial Formulation 1997 for the Thermodynamic Properties of Water and Steam, Technical Report, Erlangen, Germany, 1997. URL: www.iapws.org/relguide/IF97-Rev.pdf.

[24] M. Sharqawy, Thermophysical properties of seawater: A review of existing correlations and data, Desalin Water Treat 16 (2010) 354–380.

[25] V. Dhir, J. Lienhard, Laminar Film Condensation on Plane and Axisymmetric Bodies in Nonuniform Gravity, J Heat Trans 1 (1971) 97–100.

[26] F. P. Incropera, T. L. Bergman, D. P. DeWitt, A. S. Lavine, Principles of heat and mass transfer, 7 ed., John Wiley & Sons, Hoboken, NJ, 2012.

[27] J. C. Chato, Laminar condensation inside horizontal and inclined tubes, ASHRAE J 4 (1962) 52–60.

[28] J. Fernández-Seara, A. A. Pardiñas, Refrigerant falling film evaporation review: Description, fluid dynamics and heat transfer, Appl Therm Eng 64 (2014) 155–171.

[29] V. Sernas, Heat transfer correlation for subcooled water films on horizontal tubes, J Heat Trans 101 (1979) 176–178.

[30] J. Rogers, S. Goindi, M. Lamari, Turbulent falling film flow and heat transfer on horizontal tube, in: Proc. of the National Heat Transfer Conference, Portland, 1995, pp. 3–12.

[31] J. Bonilla, S. Dormido, F. E. Cellier, Switching moving boundary models for two-phase flow evaporators and condensers, Commun Nonlinear Sci Numer Sim (2014).

[32] F. W. Dittus, L. M. K. Boelter, Heat transfer in automobile radiators of the tubular Type, Int Commun Heat Mass Transf 12 (1985) 3–22.

[33] Dassault Systemes, Dymola 2015 - Dynamic Modeling Laboratory, 2014. URL: www.3ds.com.

[34] L. R. Petzold, A description of DASSL: a Diferential/Algebraic System Solver, Scientific Computing (1983) 65–68.

[35] A. Pfeiffer, Optimization Library for Interactive Multi-Criteria Optimization Tasks, in: Proc. 9th International Modelica Conference, Munich, Germany, 2012, pp. 669–680.

Nomenclature

A	Area (m^2)
Ar	Archimedes number (dimensionless)
C_p	Specific heat capacity at constant pressure ($J \cdot kg^{-1} \cdot K^{-1}$)
D_i	Internal diameter (m)
F	Apparent wet area fraction (dimensionless)
g	Gravitational acceleration ($m \cdot s^{-2}$)
H	Enthalpy (J)
h	Specific enthalpy ($J \cdot kg^{-1}$)
L	Latent heat of vaporization ($J \cdot kg^{-1}$)
m	Mass (kg)
N	Number (dimensionless)
Nu	Nusselt number (dimensionless)
n	Nusselt correlation coefficient (dimensionless)
K	Mass gas constant ($J \cdot K^{-1} \cdot kg^{-1}$)
k	Thermal conductivity ($W \cdot m^{-1} \cdot K^{-1}$)
Pr	Prandl number (dimensionless)
p	Pressure (Pa)
Q	Heat (J)
Re	Reynols number (dimensionless)
r	Radius (m)
S	Salinity, salt mass fraction (dimensionless)
T	Temperature (K)
V	Volume (m^3)
y	Proportional number (dimensionless)
Greek symbols	
α	Heat transfer coefficient ($W \cdot m^{-2} \cdot K^{-1}$)
μ	Dynamic viscosity ($kg \cdot m^{-1} \cdot s^{-1}$)
ν	Kinematic viscosity ($m^2 \cdot s^{-1}$)
ρ	Density ($kg \cdot m^{-3}$)
Subscripts	
av	Average
bc	Horizontal tube bundle condenser
c	Falling film condenser
col	Column
cond	Condensate
e	Falling film evaporator
ev	Evaporated
ff	Falling film evaporator or condenser
fl	Flash
fs	Feed seawater
g	Gas volume
hw	Hot water
in	Inlet
mea	Measured
mix	Mixer
out	Outlet
p	Presure flow
par	Parallel pipes
pp	Pipe
row	Row
sim	Simulated
sl	Saturated liquid
sv	Saturated vapor
w & w2	Pipe wall
water	Water

Newton's notation is used for time derivatives.

Table 1: Design specification of PSA-MED plant [11]

Number of effects	14
Heat source energy consumption	200 kW
Performance ratio	>9
Hot water flow rate	12 L/s
Feed seawater flow rate	8 m^3/h
Brine reject	5 m^3/h
Distillate production	3 m^3/h
Top brine temperature	68°C
Condenser temperature	33°C
Vacuum system	Hydroejectors (seawater at 3bar)

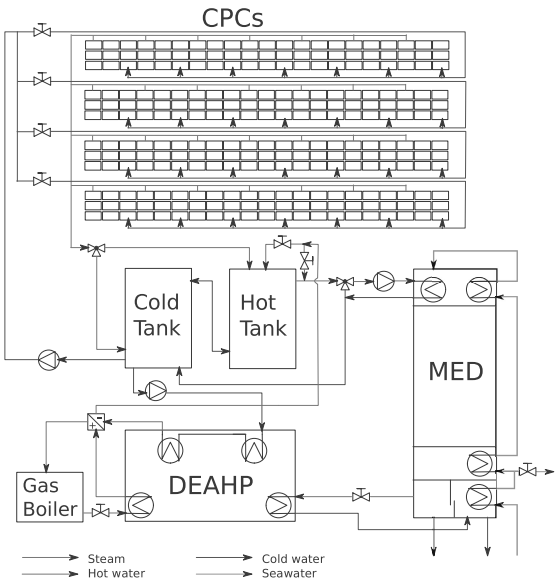

Figure 1: AQUASOL project plant flow sheet

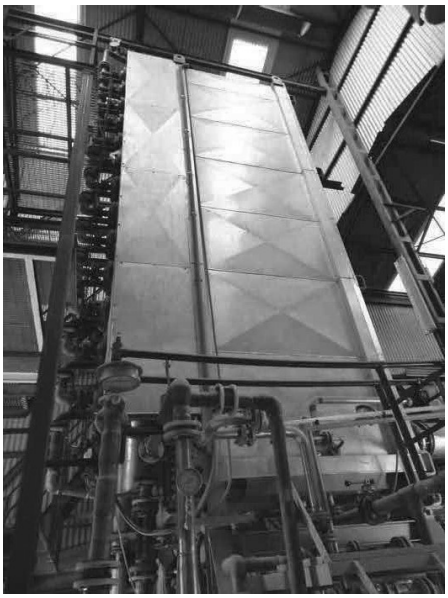

Figure 2: MED plant at PSA

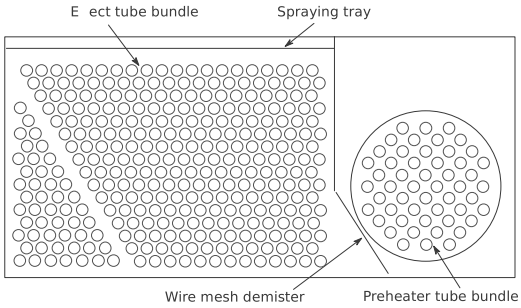

Figure 3: Cross-sectional view of a cell

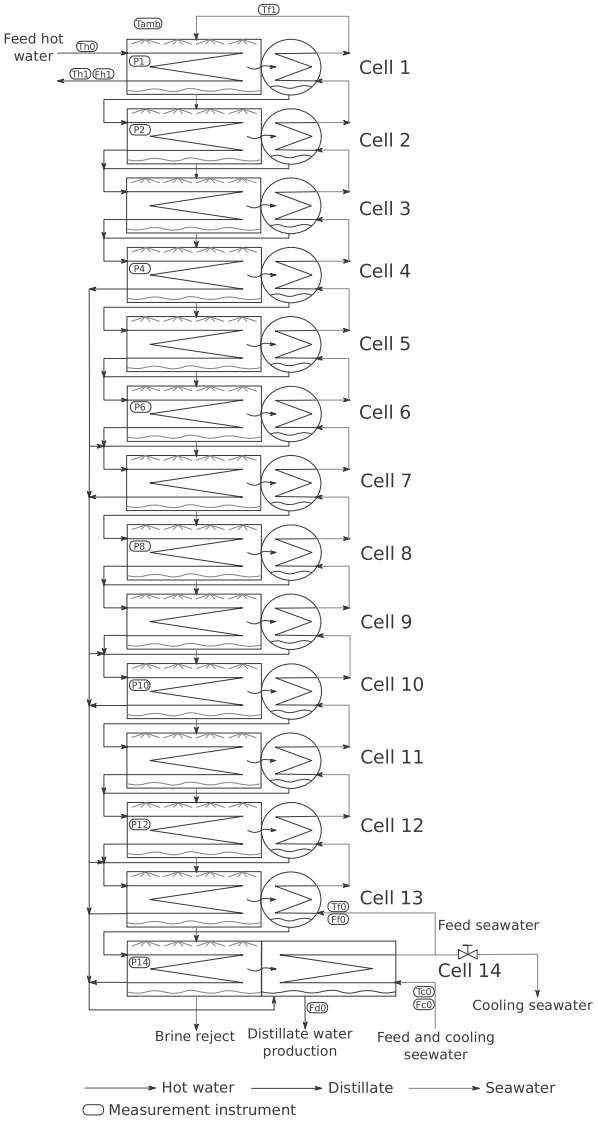

Figure 4: Schematic diagram of the MED plant at PSA

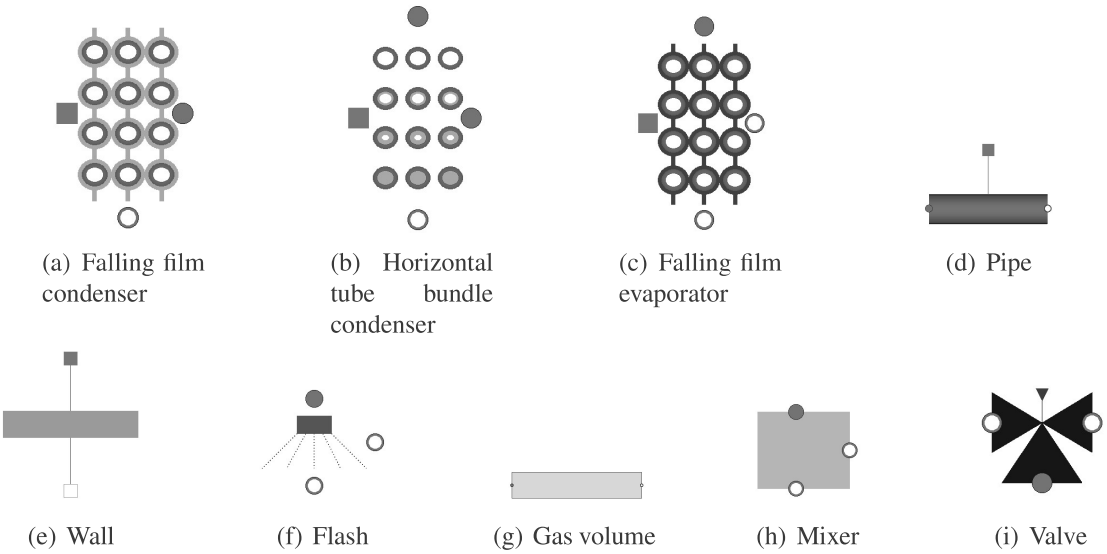

(a) Falling film condenser

(b) Horizontal tube bundle condenser

(c) Falling film evaporator

(d) Pipe

(e) Wall

(f) Flash

(g) Gas volume

(h) Mixer

(i) Valve

Figure 5: Low level models

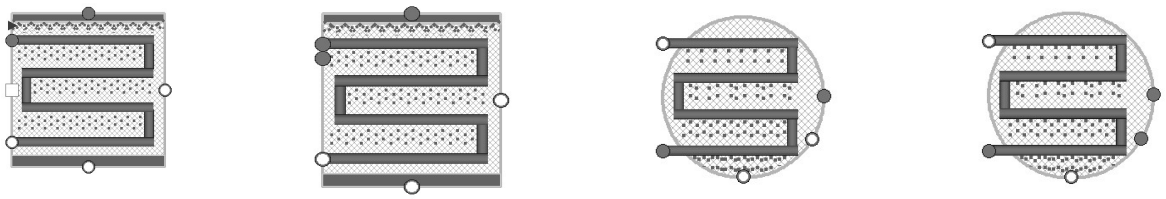

(a) Heater (b) Effect (c) Preaheater (d) Condenser

Figure 6: Medium level models

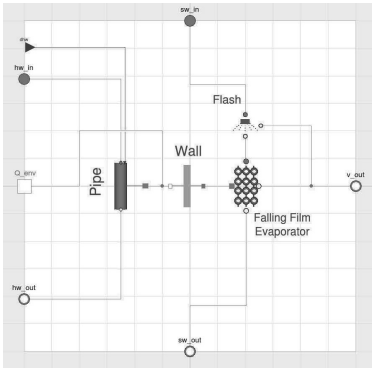

(a) Heater

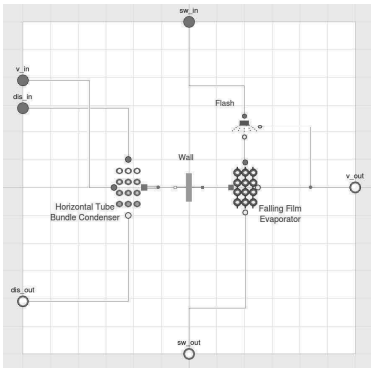

(b) Effect

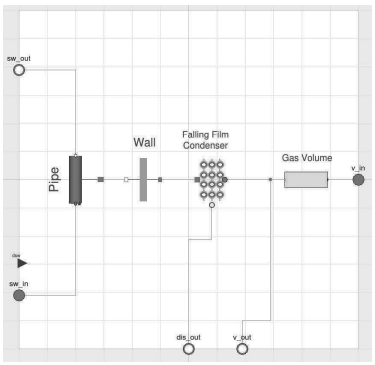

(c) Preaheater

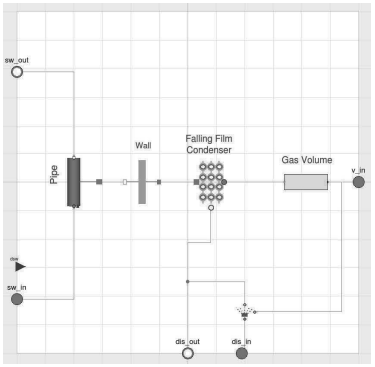

(d) Condenser

Figure 7: Medium level encapsulations

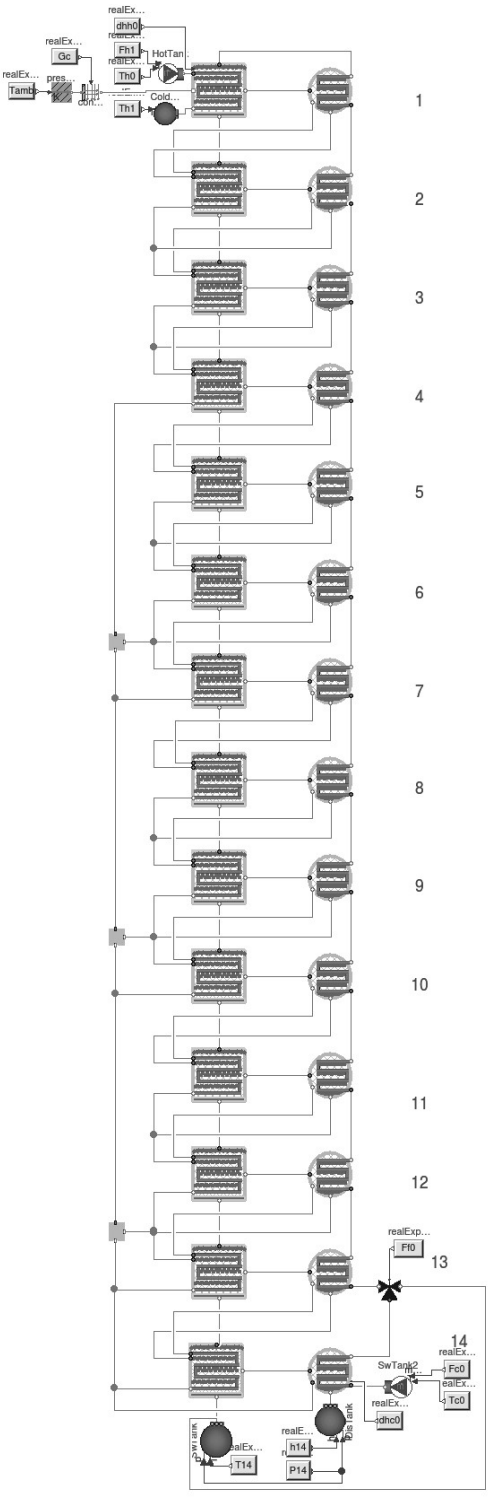

Figure 8: High Level Model

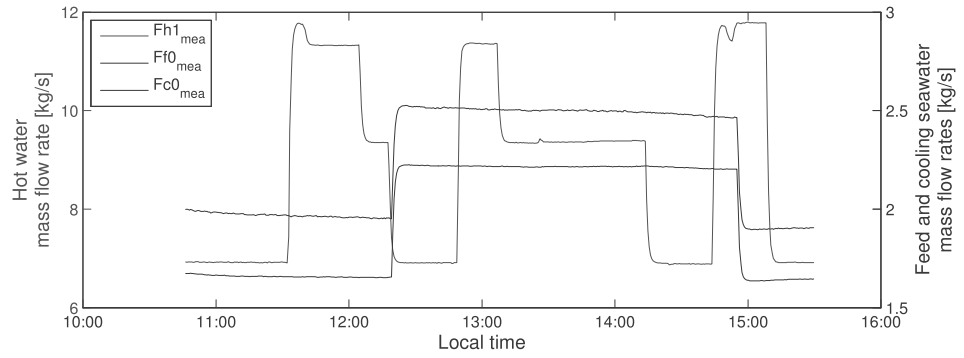

(a) Inlet mass flow rates

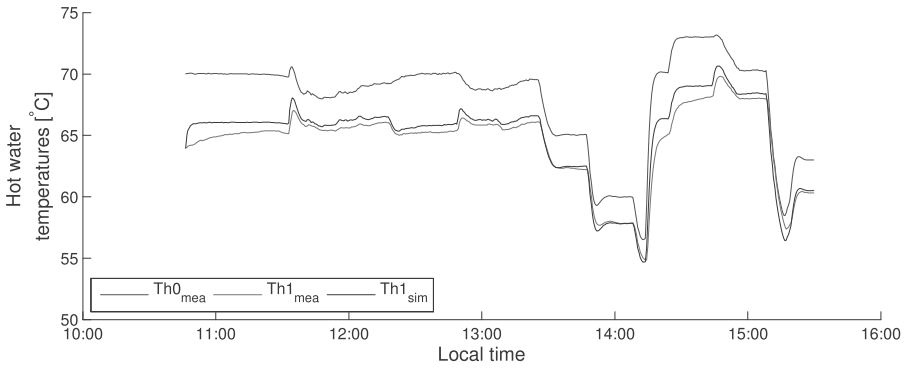

(b) Inlet and outlet hot water temperatures

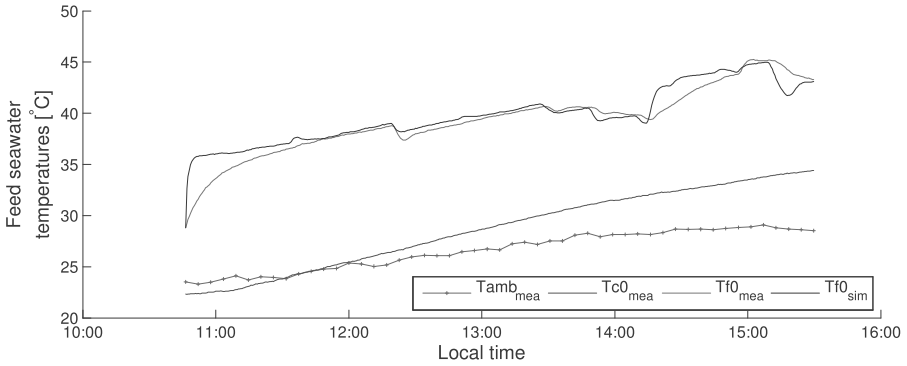

(c) Inlet and outlet feed and cooling seawater temperatures

Figure 9: Inlets and outlets of the model

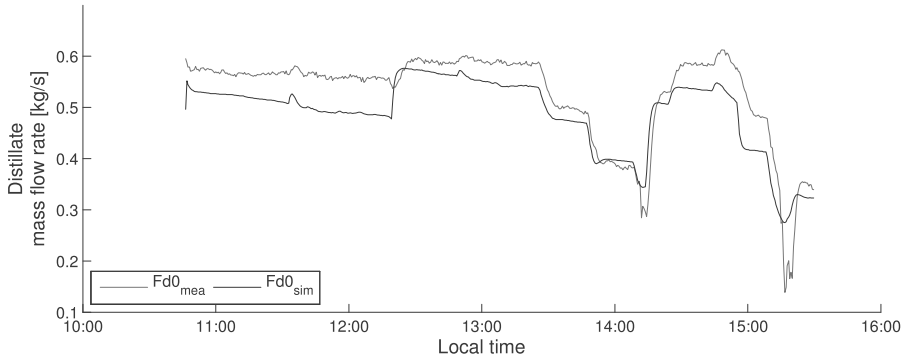

(a) Distillate mass flow rate

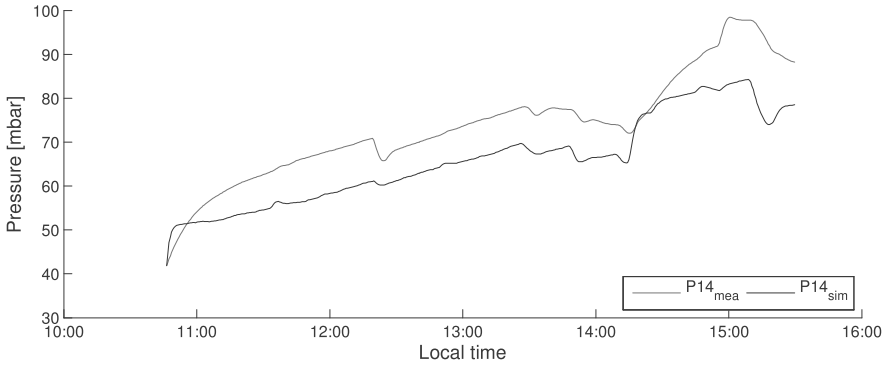

(b) Final condenser pressure

Figure 10: Inlets and outlets of the model II